Cement and Concrete Composites 153 (2024) 105715

Contents lists available at ScienceDirect

Cement and Concrete Composites

journal homepage: www.elsevier.com/locate/cemconcomp

Microstructure development of calcium carbonate cement through polymorphic transformations

Craig W. Hargis [a,*], Irvin Chen [a], Ying Wang [a], Hamed Maraghechi [a], Ryan J. Gilliam [a], Paulo J.M. Monteiro [b]

[a] Fortera Corporation, 100 Great Oaks Blvd, CA 95119, USA
[b] Department of Civil and Environmental Engineering, University of California, 760 Davis Hall, Berkeley, CA 94720, USA

ARTICLE INFO

Keywords:
Calcium carbonate
Vaterite
Aragonite
Calcite
Microscopy
Microtomography
Cement

ABSTRACT

This study presents the mechanical properties and polymorphic transformation of pastes made with calcium carbonate cement, where vaterite was the main component. Both laboratory (compression tests, XRD, & SEM) and synchrotron-based techniques (transmission X-ray microscopy and microtomography) were used in the characterization of the pastes. Mechanical properties were developed by controlling the polymorphic transformation of vaterite. When converting to aragonite, calcium carbonate cement exhibited three times greater strength development compared to its conversion to calcite at a water-to-cement ratio of 0.4, which resulted in 42 % porosity. During the conversion to aragonite, the calcium carbonate cement paste develops an interpenetrating matrix of aragonite needles that enhance strength development through interlocking at a low paste bulk density of 1.6 g/cm^3. Together the environmental and mechanical properties of calcium carbonate cement suggest its potential as a greener building material compared to traditional Portland cement.

1. Introduction

Responsible for 7–8 % of all anthropogenic CO_2 emissions, over 3 % of global energy demand, and more than 5 % of global anthropogenic particulate matter emissions, Portland cement production poses significant environmental challenges [1]. It is imperative to adopt mitigation applications to address these issues in the face of increasing global population and urbanization. In recent years, a range of technical measures has emerged to alleviate these environmental impacts. For instance, carbonation curing, secondary chemical reactions for carbon capture, geological storage, etc. Can harness the CO_2 present in waste gases from cement kilns and fossil fuel incinerators [2]. Nevertheless, these measures often encounter technical and economic challenges when applied in cement plants. An alternative approach to effectively reduce CO_2 emissions within the cement industry involves diminishing the required Portland cement quantities by utilizing supplementary cementitious materials (SCMs) or fillers in blended cement with optimized mixture designs [2] or creating a new type of low-carbon or zero-carbon emission binder.

Calcium carbonate is an abundant natural resource that exists as various types of minerals in the Earth's crust and a key component of marine ecosystems largely found in shells, corals, and skeletons of marine organisms. It has also long been utilized in civil engineering. Calcium carbonate has been used directly in the form of quarried blocks to form architectural columns and walls, crushed to form aggregate to be mixed in concrete, burned in kilns to make lime and cement, interground with clinker as a reactive extender, co-substituted for clinker along with calcined clay in LC^3 mixes [3–5], combined with coal ash or other pozzolans in blended cements [6,7], or used to make self-compacting concrete [8–11]. Calcium carbonate has also been investigated as a precipitated material by chemical engineers for its potential uses in paper, paint, thermoplastics, and rubber [12,13]. Additionally, calcium carbonate has been investigated as a medical cement for bone substitution and repair [14–16] and explored on the pilot scale as a novel low-carbon footprint cement and cement replacement to be used in the construction industry [17–20].

Calcium carbonate has three anhydrous polymorphs: vaterite, aragonite, and calcite. Amorphous calcium carbonates are produced at early ages from precipitation reactions carried out at high supersaturation conditions and will crystallize into lower energy polymorphs with

* Corresponding author.
E-mail addresses: chargis@forterausa.com (C.W. Hargis), irvinachen@gmail.com (I. Chen), hmaraghechi@calportland.com (H. Maraghechi), rgilliam@forterausa.com (R.J. Gilliam), monteiro@berkeley.edu (P.J.M. Monteiro).

https://doi.org/10.1016/j.cemconcomp.2024.105715
Received 3 June 2024; Received in revised form 14 August 2024; Accepted 17 August 2024
Available online 21 August 2024

time [12,21]. Calcite is the thermodynamically stable phase of calcium carbonates at ambient temperature and pressure, and vaterite and aragonite are metastable. Vaterite and aragonite may convert to lower energy polymorphs either through a dissolution and precipitation process in an aqueous environment [22] or with elevated temperature in the solid state on heating above 600 K [23]. Several factors have been identified that alter which calcium carbonate polymorph preferentially forms, including temperature, degree of supersaturation, pH, and accompanying ions in the solution [24–26]. Calcite tends to form at high pH, low temperature, and low supersaturation conditions [25]. Aragonite preferentially forms at moderately elevated temperatures (60–80 °C) or in the presence of Mg ions [24,27,28]. Vaterite is the predominant phase initially crystallized at low pH and high supersaturation conditions. The addition of organic solvents, such as dimethyl sulfoxide (DMSO), methanol, or isopropanol, can also influence the rate of precipitation, as well as the type and characteristics of the polymorphs [26]. Each of the different calcium carbonate polymorphs formed by the precipitation reactions shows a different principal morphology. Generally, calcite grows to form rhombs, aragonite has an acicular habit, and vaterite forms agglomerated spheres (framboids) when precipitated from solutions of sodium carbonate and calcium chloride (aka double salt precipitation method) [29,30] and agglomerated spheres of lenses when precipitated from ammonium-bearing solutions [19,20,26,31].

Portland cement achieves its long-term strength gain primarily through the hydration reactions of calcium silicates. This process results in the formation of space-filling calcium silicate hydrates characterized by high surface areas, which generate substantial forces via secondary bonding, and the development of disordered structures with polymerized silicate linkages, creating strong covalent bonds [32]. However, many cementing systems rely on the interlocking of crystals to gain strength, for instance, gypsum plaster and cements containing high amounts of calcium sulfoaluminate [33,34]. In the case of calcium sulfoaluminate reactions, one of the principal reaction products (ettringite) is acicular, and needles that began in different regions have been shown to interpenetrate [34]. This interpenetration of needles could significantly contribute to the strength gain of the system. It is then a plausible hypothesis that if vaterite at its higher energy state and spherical morphology were allowed to dissolve and precipitate out as aragonite, then aragonite's acicular shape would produce significant interpenetration and strength development, even in low-density cement pastes; moreover, it would be expected that if the calcium carbonate precipitated as calcite instead, then the rhombs would have less effective interlocking which would result in lower strength in low-density cement pastes.

This study investigated the polymorphic transformation of calcium carbonate cement [35] from vaterite to aragonite and/or calcite with particular emphasis on the microstructure development and how that affects the strength of the resulting hardened pastes.

2. Materials and methods

2.1. Materials

The calcium carbonate cement (CcC) utilized in all experiments was produced by the double salt precipitation method using 0.3M $CaCl_2$ and 0.6 M Na_2CO_3 in a 250 L continuous flow stirred tank reactor. Equation (1) provides the CcC synthesis reaction. It has a mean particle size of 22.4 μm with a standard deviation of 7.3 μm, which was determined using laser diffraction (Horiba Partica LA-950) with refractive indices of 1.58 and 1.378 for calcium carbonate and isopropanol, respectively. Fig. 1 shows the particle size distribution of the CcC. The CcC was a mixture of 80.0 % vaterite and 20.0 % calcite as determined by quantitative X-ray diffraction (XRD) (PANalytical X'Pert Powder with X'Celerator detector) utilizing a 2-h continuous scan from 5.0 to 75.0° 2θ with a monochromatic Cu Kα wavelength of 1.5418 Å. Rietveld analysis was performed using Materials Analysis Using Diffraction (MAUD) software. The XRD pattern of the CcC utilized is shown in Fig. 2. The CcC displays the typical morphology of rhombohedral calcite and framboidal vaterite under scanning electron microscopy (SEM) as shown in Fig. 3.

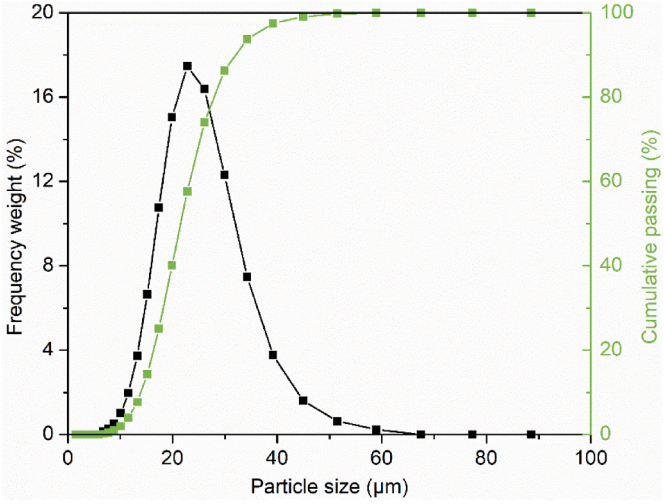

Fig. 1. Particle size distribution of the raw powder of CcC.

$$CaCl_2 + Na_2CO_3 \rightarrow 2NaCl + CaCO_3\ (CcC;\ 80\%\ vaterite\ \&\ 20\%\ calcite) \quad (1)$$

2.2. Methods

The hypothesis posited that the acicular morphology of aragonite would confer increased strength to hardened cement pastes compared to rhombohedral-shaped calcite at low paste densities, owing to the mechanical interlocking of aragonite needles. To assess this hypothesis, two sets of samples were prepared. In the first set, CcC was combined with deionized water to induce the transformation to calcite, and these samples were designated as CcC-C. In the second set, a 1.5 wt % $MgCl_2$ solution was employed to convert vaterite to aragonite, and these samples were labeled CcC-A.

Cement paste cubes (5.08 cm [2 in.]) of CcC were produced using a liquid (solution or water) to cement mass ratio (w/c) of 0.4. The pastes

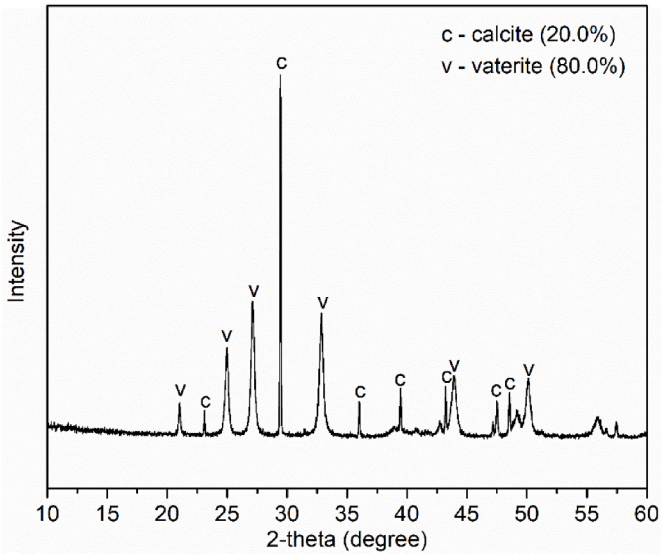

Fig. 2. XRD characterization of the raw powder of CcC.

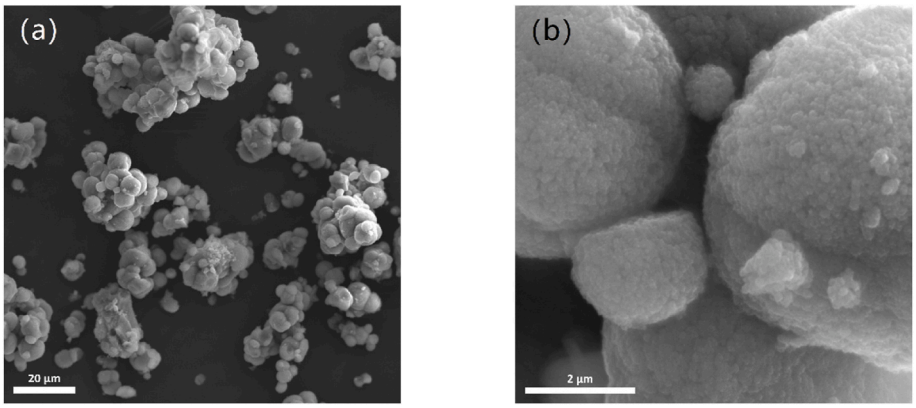

Fig. 3. SEM images showing the morphology of anhydrous CcC: (a) Agglomerated framboidal vaterite; (b) Close-up image of framboidal vaterite surface showing nano-sized primary crystallites.

were mixed and molded following ASTM C305. Subsequently, the samples were placed in a chamber at 100 % relative humidity and 60 °C until demolding. The 60 °C temperature was selected to accelerate the CcC reactions [31]. CcC-C samples were demolded after 5 days, while CcC-A samples underwent demolding after 12 h, 1 day, and 5 days curing. After demolding, the samples were stored in a drying oven at 105 °C for approximately 4 h until a constant mass was attained to arrest the cementing reactions. Compression tests were then conducted on 3 cubes per testing age in accordance with ASTM C109.

SEM was utilized to image the raw CcC powder and the fracture surfaces of hardened cement pastes. The samples were coated in Au/Pd for secondary electron imaging. The SEM used was a Zeiss EVO MA10® utilizing a 15 kV accelerating voltage and 30 pA beam current.

Soft X-ray microscopy was utilized to observe the early-age transformation of the calcium carbonate cement. The microscope was operated in the water window (around 2.4 nm photon wavelength) to provide high lateral resolution (few tens of nm range) with the ability to penetrate several μm of aqueous solution, which makes it an ideal in-situ technique to study wet nanostructured materials. In-situ experiments, resulted in too many artifacts, such as rapid dissolution at the observation site or crystallization of the $MgCl_2$ solution, so ex-situ observations were made by stopping transformation by solvent exchange with isopropyl alcohol, followed by a brief drying period in an oven to remove the isopropyl alcohol. The dry sample was then placed on a TEM grid and imaged. The X-ray optical setup of the soft X-ray microscope, XM-1, which is operated at the Advanced Light Source in Berkeley, CA is described elsewhere [36].

Microtomography experiments were conducted with synchrotron-produced X-rays at Beamline 8.3.2 of the Advanced Light Source with an energy of 38 keV at a ring current of 500 mA. MacDowell et al. [37] give the beamline's setup. The present experiments utilized a 20x lens resulting in a pixel size of 0.325 μm and a field of view of 0.8 mm. One paste cylinder with a diameter of 0.7 mm for CcC-A and CcC-C was cast, cured, and dried using the same procedure as that applied to the cubes.

3. Results

3.1. Strength and phase transformation

Fig. 4 shows the enthalpy changes associated with transforming vaterite to aragonite and calcite [38–40]. The notably higher energy state of vaterite in comparison to aragonite and calcite facilitates the dissolution-reprecipitation process following the mixing of vaterite with water or a solution. The elevated energy level of vaterite creates favorable conditions for its breakdown and subsequent reformation into more stable phases.

Fig. 5 shows the XRD patterns comparing the raw CcC powder and

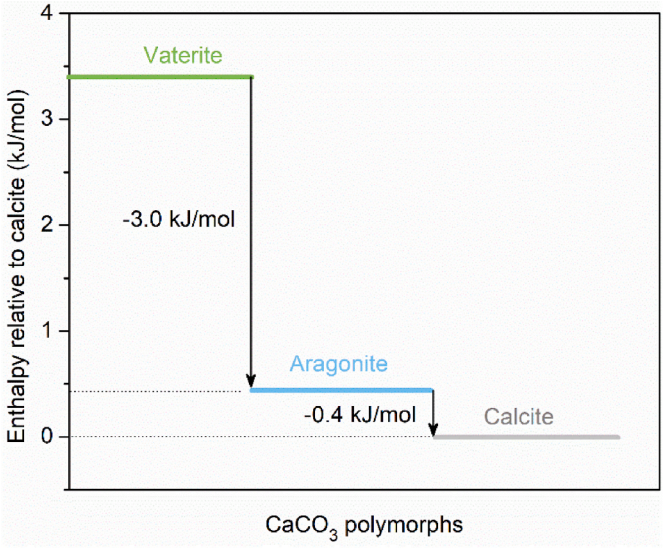

Fig. 4. Relative energetic stabilities of vaterite and aragonite with respect to calcite.

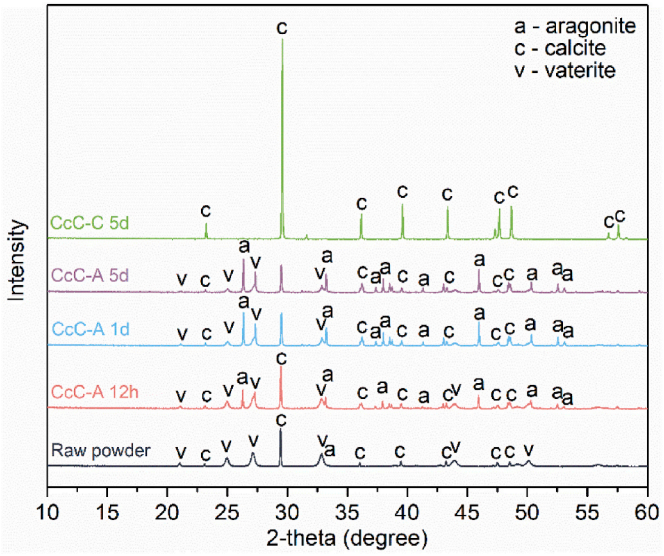

Fig. 5. XRD patterns of the raw CcC powder and the paste samples at different ages.

the paste samples at different ages. Fig. 6 illustrates the compressive strength and phase evolution of CcC over time. The initial composition of CcC was 80 % vaterite and 20 % calcite. CcC-A samples, mixed with a 1.5 wt% $MgCl_2$ solution when casting, exhibited a progressive transformation from vaterite to aragonite, reaching 32 %, 46 %, and 51 % aragonite at 0.5, 1, and 5 days of curing, respectively. Notably, the calcite percentage in CcC-A remained relatively stable, with aragonite being the predominant conversion product. The compressive strength of CcC-A demonstrated a rapid increase up to 1 day, after which there was no significant change (the difference in strengths at 1 and 5 days are within the error bars), despite an additional 5 % vaterite transformation. In contrast, CcC-C samples, mixed with deionized water during casting, completed the conversion to calcite after 5 days. CcC-C exhibited a compressive strength of approximately 30 % that of CcC-A at a w/c = 0.4.

3.2. Microscopy

Fig. 7a, b, and 8a show fracture surfaces of CcC-A at 5 days. Aragonite needles surround partially dissolved vaterite spheres. The vaterite spheres produced via the double salt method dissolve heterogeneously, often forming pits from the center instead of dissolving from the outside inward as is common for Portland cement hydration. Broken shells of vaterite spheres can be seen in Fig. 7a and b, and the outer surface of a vaterite sphere residing on the surface of an air void can be seen in Fig. 8a. The partially dissolved vaterite spheres have an etched appearance from dissolution. Aragonite needles grow on the surfaces of the vaterite spheres creating a matrix of interlocking needles that cement the vaterite spheres together.

Fig. 8b shows a transmission X-ray microscope image of the calcium carbonate cement transforming to aragonite, CcC-A, at 4.5 h. Fine nanometer-sized aragonite needles can be seen growing on the surface of the lower vaterite sphere. Aragonite nucleating on the surface of vaterite during the transformation of vaterite to aragonite is consistent with prior observations. Nielsen et al. [29] hypothesized that the higher mobility of surface ions and their ability to exchange with the surrounding solution promoted initial aragonite formation on the surface of the dissolving vaterite. Additionally, larger crystals can be seen bridging between the adjacent vaterite spheres.

Fig. 9a shows the calcite matrix of CcC-C at 5 days, and Fig. 9b shows a magnified view of the calcite bridge in the center of Fig. 9a. Calcite predominately occupies the space between where the vaterite spheres would have been (the space initially occupied by mixing water), leaving

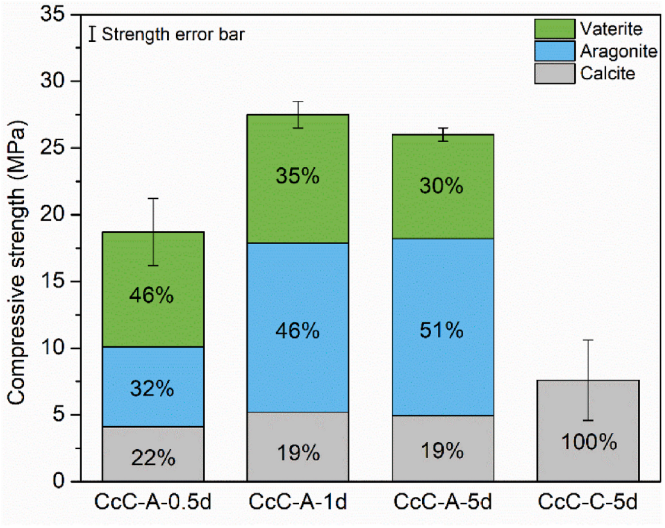

Fig. 6. Strength development and mineral composition of CcC-A and CcC-C through 5 days of curing.

spherical negatives of the dissolved vaterite spheres. The calcite rhombs grow together but, due to their rhombohedral crystal habit, do not interpenetrate deeply like the aragonite crystals in CcC-A. The much higher strength of the CcC that converts to aragonite instead of calcite supports the hypothesis that networks of interpenetrating acicular reaction products can significantly contribute to the strength development of inorganic cements at low paste densities.

3.3. Microtomography

Fig. 10 shows the transformation of the CcC to aragonite or calcite imaged by microtomography. In the unreacted CcC (Fig. 10a), vaterite and calcite can be differentiated because they have different densities. Calcite (2.71 g/cm^3) appears light gray, vaterite (2.55 g/cm^3) appears gray, and the charcoal in between is porosity.

At 12 h in solution, the CcC has begun to dissolve and precipitate as aragonite (Fig. 10b). Many small vaterite spheres have completely dissolved leaving only their outlines covered in an aragonite matrix. The larger vaterite spheres show interesting patterns of dissolution with dissolving pits forming from the center, instead of dissolving from the outside inward. The vaterite spheres can be seen to be losing density (evidenced by their darker gray appearance in regions) before fully dissolving away. This is consistent with the SEM fracture surfaces that show signs of etching on the interior of the vaterite spheres in Fig. 7. As dissolution progresses, the spaces previously occupied by vaterite become pores with a few aragonite needles penetrating through them, and the space between the vaterite spheres becomes filled with aragonite needles forming an interconnecting matrix, as shown in Fig. 10c and d.

Fig. 10e shows the transformation of CcC in water, CcC-C at 5 days. The hardened cement paste develops an interconnected matrix; however, in tomography, that matrix appears more compact and less fibular, which corresponds to the more compact rhombohedral structure of calcite observed in the SEM images in Fig. 9.

Fig. 11 shows 3D renderings of CcC-A at 12 h and 1 day and CcC-C at 5 days. As observed in the tomography slice images, the cement paste becomes more interconnected over time resulting from the interpenetration of aragonite needles binding the material together. Analyzing the pore structure of both CcC-A and CcC-C reveals that the porosity of the packed CcC before transformation and the hardened pastes are all approximately equal (42 ± 3 %) indicating the majority of the porosity is set by the volume of the liquid in the mix. This is important because if the amount of liquid in the mix can be reduced, then the porosity of the hardened cement pastes will decrease, resulting in increases in strength and decreases in permeability. Decreasing the liquid in the mix could be achieved by using water-reducing admixtures, improved particle packing (apollonian packing), or pressing the plastic pastes.

Utilizing the w/c ratio and a density of 2.55 g/cm^3 for CcC, a theoretical paste porosity can be calculated to be 51 %, assuming the paste does not change in volume after casting. The difference between observed and calculated porosity would indicate consolidation of the CcC paste after casting, in other words bleeding or loss of liquid volume. Using the measured porosity from microtomography, the phase composition of CcC-A at 5 days, and the densities of the phases, a dry bulk density of the paste can be calculated to be 1.61 g/cm^3. Portland cement paste at a w/c = 0.4 has a density of approximately 2.35 ± 0.05 g/cm^3 [41]. Comparing the density of a Portland cement paste at a w/c = 0.4 shows the CcC-A paste is approximately 30 % lighter. Additional image analysis shows that ≥99 % of the porosity of CcC-A and CcC-C is interconnected at all ages.

4. Discussion

This study demonstrated that calcium carbonate in the form of framboidal vaterite shows enhanced cementitious characteristics at a low paste density, such as higher paste cube strength and matrix

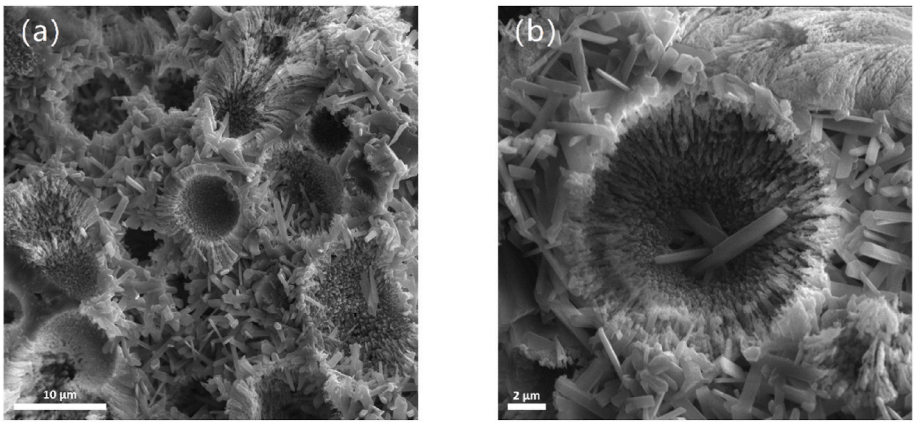

Fig. 7. SEM images of fractured surfaces of CcC-A at 5 days: (a) Field of interlocking aragonite needles and dissolved vaterite cores; (b) Close-up image of dissolving vaterite sphere surrounded and penetrated by aragonite needles.

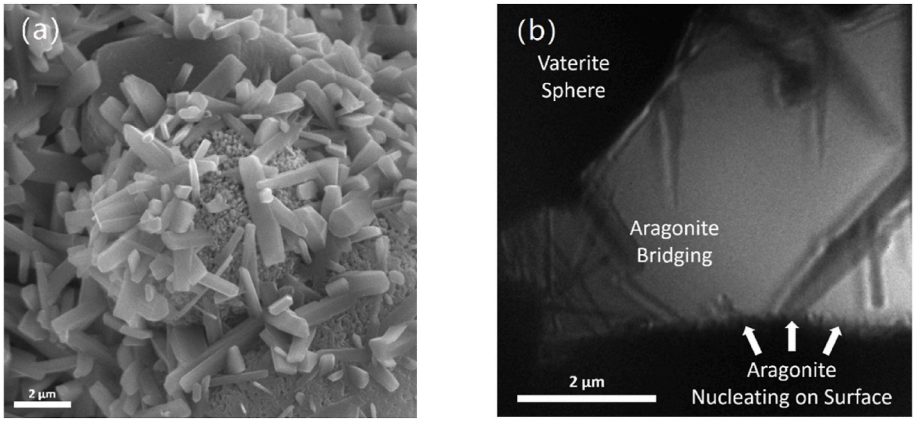

Fig. 8. (a) SEM image of vaterite sphere with aragonite on its surface in an air void of CcC-A at 5 days; (b) Transmission X-ray microscopy image of CcC-A at 4.5 h.

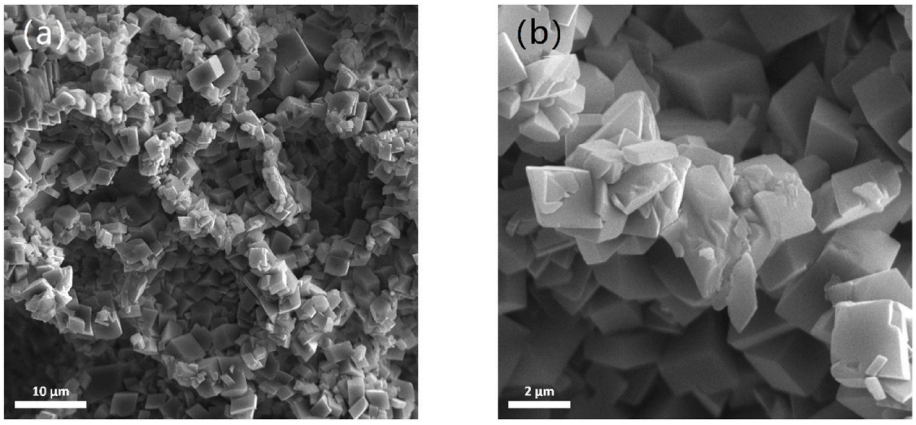

Fig. 9. SEM images of fractured surfaces of CcC-C at 5 days: (a) Calcite bridging network around empty spaces previously occupied by vaterite; (b) Higher magnification image of calcite bridge.

complexity, contingent to conversion to aragonite (through dissolution precipitation reactions) as the main polymorph, instead of calcite. The mechanism of microstructure formation for different calcium carbonate polymorphs and their influence on physical and mechanical properties were also investigated.

In a controlled aqueous environment (e.g., right pH, temperature, and presence of specific ions), the double salt precipitated vaterite spheres start etching and dissolving from within, followed by the formation of acicular aragonite crystals on the surface of the vaterite spheres, generally leaving a semi-hollow core behind. While most aragonite needles tend to grow outward due to higher space availability and lower constraints, some can grow inwards within the dissolving vaterite.

The compressive strength of CcC pastes was measured to be at least 3.5 times higher after aragonite formation/precipitation compared to calcite precipitation at a w/c = 0.4. The enhanced strength at low density is mainly due to the interlocking and interpenetration of aragonite's orthorhombic crystals with acicular morphology. Unlike

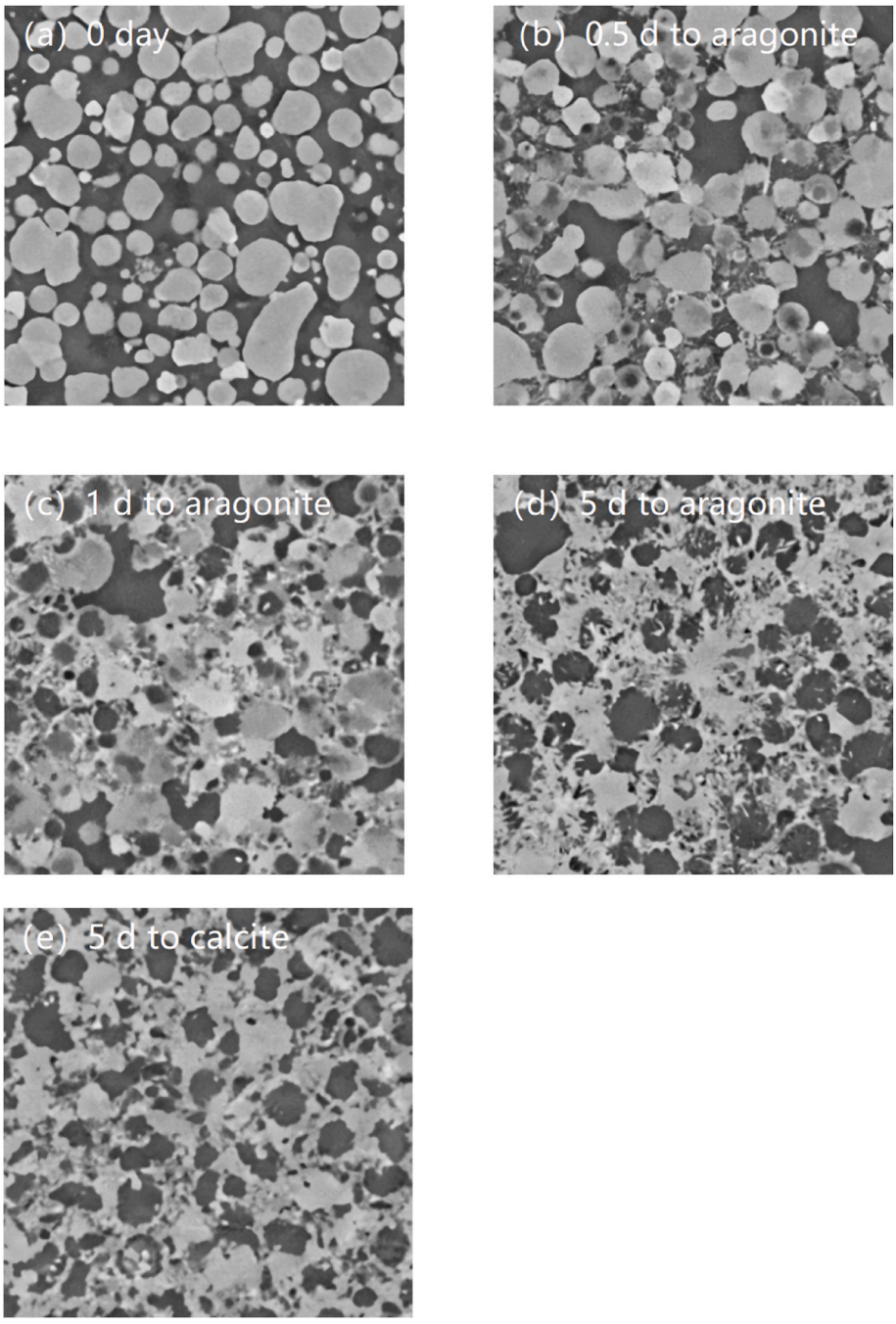

Fig. 10. Microtomography slices of (a) CcC; (b) CcC-A 12 h; (c) CcC-A 1 day; (d) CcC-A 5 days; (e) CcC-C 5 days. The field width is 163 μm.

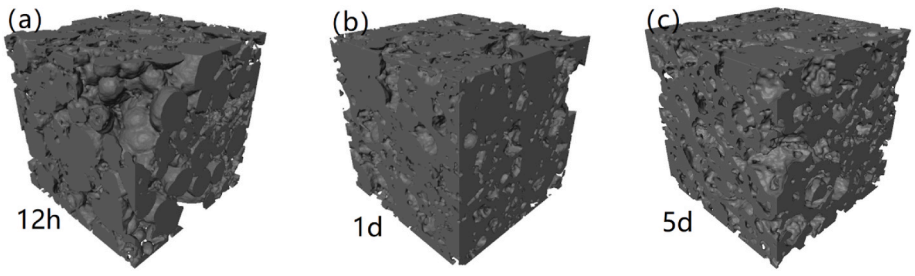

Fig. 11. 3D microtomography rendering of (a) CcC-A at 12 h; (b) CcC-A at 1 day; (c) CcC-C at 5 days. Cube edges are 81 μm.

aragonite, the rhombohedral shape of calcite crystals does not provide such interlocking characteristics at low densities. Similar crystal interlocking mechanisms contributed to strength gain in calcium sulfoaluminate cements, where needle-like ettringite crystals form and interpenetrate [34]. Likewise, gypsum ($CaSO_4{\cdot}2H_2O$) products upon precipitation after the dissolution of calcium sulfate hemihydrate ($CaSO_4{\cdot}½H_2O$, plaster of Paris) can form rod-like crystals with an interlocking morphology [42,43].

The formation of aragonite and inhibition of calcite can be controlled using magnesium-based additives (e.g., $MgCl_2$, $MgSO_4$, $Mg(C_2H_3O_2)_2$) [27,28]. The size and aspect ratio of the acicular aragonite may also be controlled using strontium-based additives (e.g., $SrCl_2$, $Sr(C_2H_3O_2)_2$), which are known to promote aragonite formation [28]. After vaterite transformation to aragonite, further transformation from aragonite to calcite has not been observed in CcC pastes or mortars, even in simulated leaching experiments. This could be due to the low energy difference between aragonite and calcite and/or the chemistry of the hardened aragonite matrix.

Calcium carbonate cement presents a versatile option for manufacturing diverse building products, including concrete roof tiles, stone veneer, concrete blocks, autoclaved aerated concrete, decorative concrete, and fiber cement boards, products traditionally crafted from Portland cement or gypsum. Utilizing calcium carbonate cement offers several advantages, such as expedited production, a significantly reduced carbon footprint due to no chemical emission of CO_2 during manufacturing CcC, a pure white color, and a lighter overall weight [31]. These benefits position CcC as an environmentally conscious and efficient alternative in the construction materials industry.

It should be noted that there is no permanent binding of water in the calcium carbonate cementing process, and water is used as a dissolution/precipitation medium and can be fully recovered in a closed-loop manufacturing setting. This could provide additional environmental benefits to manufacturers in regions with water scarcity.

Furthermore, upon drying the transformed mixtures, interconnected micro/macro porosity is formed. While this may be a concern in some applications where water or ion transport could occur, different methods, such as improving particle size distribution characteristics of concrete constituents or using water reducers, could be employed to achieve lower porosity and higher strength systems [44]. Research investigating the effect of altering CcC characteristics and the use of admixtures is ongoing and will be published in the future.

Different aspects of CcC manufacturing, such as the availability of raw materials and energy or CO_2 footprint are discussed in depth in another published article [31]. While materials such as landfilled carbide lime sludge and steel slag can be used for manufacturing CcC, the use of calcined limestone as the raw feed could provide tremendous economic and environmental opportunities to cement, concrete, and construction industries and is currently under large-scale development [45–47].

5. Conclusions

The transformation of calcium carbonate cement (CcC, 80 % vaterite) to aragonite or calcite was followed with traditional analytical techniques (XRD & SEM) and synchrotron-based techniques (transmission X-ray microscopy and microtomography) at the Advanced Light Source. Results showed that transforming CcC to aragonite instead of calcite results in approximately three times greater strength (27.5 MPa vs. 7.6 MPa) at a w/c = 0.4. Moreover, the higher strength development at low paste density results from the interpenetrating aragonite matrix formation (CcC-A) compared to the rhombohedra of the calcite matrix (CcC-C). The aragonite needles nucleate on the surface of the vaterite spheres and continue to grow and interlock as the vaterite heterogeneously dissolves. The amount of porosity of hardened calcium carbonate cement pastes is predominately set by the amount of liquid in the mix and is highly interconnected. With its white color, strength-to-weight ratio, and lower carbon footprint, CcC-formulated building materials have the potential to help the building materials industry to create lightweight building materials with reduced embodied carbon.

Funding

C.W. Hargis was supported by the Berkeley Fellowship for Graduate Study and the Carlson-Polivka Fellowship. This material is based upon work supported by the U.S. Department of Energy, Office of Fossil Energy, under Award Number DE-FE-0002472. Research at the Advanced Light Source is supported by the Director, Office of Science, Office of Basic Energy Sciences, of the U.S. Department of Energy under contract no. DE-AC02-05CH11231. We thank Peter Fischer, Mi-Young Im, Dula Parkinson, and Alastair MacDowell for assisting the users and maintaining the beamlines.

Institutional review board statement

Not applicable.

Informed consent statement

Not applicable.

CRediT authorship contribution statement

Craig W. Hargis: Writing – review & editing, Writing – original draft, Project administration, Methodology, Investigation, Formal analysis, Data curation, Conceptualization. **Irvin Chen:** Writing – review & editing, Project administration. **Ying Wang:** Writing – review & editing, Visualization. **Hamed Maraghechi:** Writing – review & editing. **Ryan J. Gilliam:** Writing – review & editing, Supervision, Resources, Funding acquisition. **Paulo J.M. Monteiro:** Writing – review & editing, Supervision, Resources, Methodology, Funding acquisition, Conceptualization.

Declaration of competing interest

The authors declare the following financial interests/personal relationships which may be considered as potential competing interests: Craig W. Hargis reports a relationship with Fortera that includes: employment and equity or stocks. Ryan J. Gilliam reports a relationship with Fortera that includes: board membership, employment, and equity or stocks. Ying Wang reports a relationship with Fortera that includes: employment and equity or stocks. Hamed Maraghechi reports a relationship with Fortera that includes: prior employment. Craig W. Hargis has patent #US20230339809A1 issued to Arelac, Inc. Ryan J. Gilliam has patent #US20230339809A1 issued to Arelac, Inc. Craig W. Hargis has patent #US20230099641A1 issued to Arelac, Inc. Ryan J. Gilliam has patent #US20230099641A1 issued to Arelac, Inc. If there are other authors, they declare that they have no known competing financial interests or personal relationships that could have appeared to influence the work reported in this paper.

Data availability

Data will be made available on request.

Acknowledgments

The authors thank their colleagues, scientific advisors, and investors for their dedicated support of the project. Appreciation for her assistance in conducting experiments is given to Terilyn Q. Nguyen.

References

[1] I.H. Shah, S.A. Miller, D. Jiang, R.J. Myers, Cement substitution with secondary materials can reduce annual global CO_2 emissions by up to 1.3 gigatons, Nat. Commun. 13 (2022) 1–11, https://doi.org/10.1038/s41467-022-33289-7.

[2] M.G. Plaza, S. Martinez, F. Rubiera, CO_2 capture, use, and storage in the cement industry : state of the art and expectations, Energies 13 (2020) 5692, https://doi.org/10.3390/en13215692.

[3] K. Scrivener, F. Avet, H. Maraghechi, F. Zunino, J. Ston, W. Hanpongpun, A. Favier, Impacting factors and properties of limestone calcined clay cements (LC^3), Green Mater. 7 (2018) 3–14, https://doi.org/10.1680/jgrma.18.00029.

[4] Y. Li, Y. Li, H. Ma, J. Li, The hydration, microstructure, and mechanical properties of vaterite calcined clay cement (VC^3), Cem. Concr. Res. 175 (2024) 107374, https://doi.org/10.1016/j.cemconres.2023.107374.

[5] C.W. Hargis, H. Maraghechi, R.J. Gilliam, Compositions, Methods, and Systems for Cement Blends with Reactive Vaterite, US 2023/0112173 A1, 2023.

[6] ASTM C595-21, Standard Specification for Blended Hydraulic Cements, Astm, 2021, pp. 1–10, https://doi.org/10.1520/C0595.

[7] I. Chen, M. Fernandez, J. Patterson, M. Devenney, Methods and compositions using calcium carbonate. https://patents.google.com/patent/US8114214B2/en, 2011.

[8] S.A. Hartshorn, J.H. Sharp, R.N. Swamy, Thaumasite formation in Portland-limestone cement pastes, Cem. Concr. Res. 29 (1999) 1331–1340, https://doi.org/10.1016/S0008-8846(99)00100-3.

[9] Z.T. Chang, X.J. Song, R. Munn, M. Marosszeky, Using limestone aggregates and different cements for enhancing resistance of concrete to sulphuric acid attack, Cem. Concr. Res. 35 (2005) 1486–1494, https://doi.org/10.1016/j.cemconres.2005.03.006.

[10] T. Matschei, B. Lothenbach, F.P. Glasser, The role of calcium carbonate in cement hydration, Cem. Concr. Res. 37 (2007) 551–558, https://doi.org/10.1016/j.cemconres.2006.10.013.

[11] K. Celik, R. Hay, C.W. Hargis, J. Moon, Effect of volcanic ash pozzolan or limestone replacement on hydration of Portland cement, Constr. Build. Mater. 197 (2019) 803–812, https://doi.org/10.1016/j.conbuildmat.2018.11.193.

[12] D. Chakraborty, V.K. Agarwal, S.K. Bhatia, J. Bellare, Steady-state transitions and polymorph transformations in continuous precipitation of calcium carbonate, Ind. Eng. Chem. Res. 33 (1994) 2187–2197, https://doi.org/10.1021/ie00033a024.

[13] W.M. Jung, S.H. Kang, W.S. Kim, C.K. Choi, Particle morphology of calcium carbonate precipitated by gas-liquid reaction in a Couette-Taylor reactor, Chem. Eng. Sci. 55 (2000) 733–747, https://doi.org/10.1016/S0009-2509(99)00395-4.

[14] M.-L. Fontaine, C. Combes, T. Sillam, G. Dechambre, C. Rey, New calcium carbonate-based cements for bone reconstruction, Key Eng. Mater. 284–286 (2005) 105–108, https://doi.org/10.4028/www.scientific.net/kem.284-286.105.

[15] C. Combes, B. Miao, R. Bareille, C. Rey, Preparation, physical-chemical characterisation and cytocompatibility of calcium carbonate cements, Biomaterials 27 (2006) 1945–1954, https://doi.org/10.1016/j.biomaterials.2005.09.026.

[16] C. Combes, S. Tadier, H. Galliard, S. Girod-Fullana, C. Charvillat, C. Rey, R. Auzély-Velty, N. El Kissi, Rheological properties of calcium carbonate self-setting injectable paste, Acta Biomater. 6 (2010) 920–927, https://doi.org/10.1016/j.actbio.2009.08.032.

[17] K. Celik, M.D. Jackson, M. Mancio, C. Meral, A.H. Emwas, P.K. Mehta, P.J. M. Monteiro, High-volume natural volcanic pozzolan and limestone powder as partial replacements for portland cement in self-compacting and sustainable concrete, Cem. Concr. Compos. 45 (2014) 136–147, https://doi.org/10.1016/j.cemconcomp.2013.09.003.

[18] C.W. Hargis, A. Telesca, P.J.M. Monteiro, Calcium sulfoaluminate (Ye'elimite) hydration in the presence of gypsum, calcite, and vaterite, Cem. Concr. Res. 65 (2014) 15–20, https://doi.org/10.1016/j.cemconres.2014.07.004.

[19] M. Devenney, M. Fernandez, I. Chen, C. Guillaume, Methods and Systems for Utilizing Carbide Lime or Slag, US, vol. 9, 2018, 902,652 B2.

[20] C.W. Hargis, R.J. Gilliam, Compositions, Methods, and Systems to Form Vaterite with Magnesium Oxide, US 2023/0099641 A1, 2022. https://patentimages.storage.googleapis.com/24/ba/b9/64edf49839fe31/US20220340486A1.pdf.

[21] L. Brečević, A.E. Nielsen, Solubility of amorphous calcium carbonate, J. Cryst. Growth 98 (1989) 504–510, https://doi.org/10.1016/0022-0248(89)90168-1.

[22] S. Kabasci, W. Althaus, P. Weinspach, Batch-precipitation of calcium carbonate from highly supersaturated solutions, Chem. Eng. Res. Des. 74 (1996) 765–772. https://api.semanticscholar.org/CorpusID:101307083.

[23] F. Baitalow, H. Schmidt, G. Wolf, Baitalow 1999, vol. 337, pdf, 1999, pp. 111–120.

[24] Y. Kitano, K. Park, D.W. Hood, Pure aragonite synthesis, J. Geophys. Res. 67 (1962) 4873–4874, https://doi.org/10.1029/JZ067i012p04873.

[25] W.-S. Kim, I. Hirasawa, W.-S. Kim, Polymorphic change of calcium carbonate during reaction crystallization in a batch reactor, Ind. Eng. Chem. Res. 43 (2004) 2650–2657, https://doi.org/10.1021/ie034161y.

[26] D. Konopacka-łyskawa, N. Czaplicka, M. Łapiński, B. Kościelska, R. Bray, Precipitation and transformation of vaterite calcium carbonate in the presence of some organic solvents, Materials 13 (2020) 1–14, https://doi.org/10.3390/ma13122742.

[27] J.L. Bischoff, Kinetics of calcite nucleation ' magnesium, J. Geophys. Res. 73 (1968) 3315–3322.

[28] J.L. Bischoff, Kinetics of calcite nucleation: magnesium ion inhibition and ionic strength catalysis, J. Geophys. Res. 73 (1968) 3315–3322, https://doi.org/10.1029/jb073i010p03315.

[29] M.H. Nielsen, S. Aloni, J.J. De Yoreo, In situ TEM imaging of $CaCO_3$ nucleation reveals coexistence of direct and indirect pathways, Science 345 (2014) 1158–1162, https://doi.org/10.1126/science.1254051.

[30] D.B. Trushina, T.V. Bukreeva, M.V. Kovalchuk, M.N. Antipina, $CaCO_3$ vaterite microparticles for biomedical and personal care applications, Mater. Sci. Eng. C. 45 (2014) 644–658, https://doi.org/10.1016/j.msec.2014.04.050.

[31] C.W. Hargis, I.A. Chen, M. Devenney, M.J. Fernandez, R.J. Gilliam, R.P. Thatcher, Calcium carbonate cement: a carbon capture, utilization, and storage (CCUS) technique, Materials (2021) 1–12.

[32] H.F.W. Taylor, Cement Chemistry, 2nd Editio, Thomas Telford Publishing, 1997, https://doi.org/10.1680/cc.25929.

[33] E.M. Gartner, Cohesion and expansion in polycrystalline solids formed by hydration reactions - the case of gypsum plasters, Cem. Concr. Res. 39 (2009) 289–295, https://doi.org/10.1016/j.cemconres.2009.01.008.

[34] C.W. Hargis, A.P. Kirchheim, P.J.M. Monteiro, E.M. Gartner, Early age hydration of calcium sulfoaluminate (synthetic ye'elimite, $C_4A_3\bar{S}$) in the presence of gypsum and varying amounts of calcium hydroxide, Cem. Concr. Res. 48 (2013) 105–115, https://doi.org/10.1016/j.cemconres.2013.03.001.

[35] B.R.I. Constantz, K. Farsad, C. Camire, U.S. Chen, Patent No. 7,922,809., U.S. Pat, 2011. No. 7,922,809. 1.

[36] W. Meyer-Ilse, H. Medecki, J.T. Brown, J.M. Heck, E.H. Anderson, A. Stead, T. Ford, R. Balhorn, C. Petersen, C. Magowan, D.T. Attwood, in: J. Thieme, G. Schmahl, D. Rudolph, E. Umbach (Eds.), X-Ray Microscopy in Berkeley BT - X-Ray Microscopy and Spectromicroscopy: Status Report from the Fifth International Conference, Würzburg, August 19–23, 1996, Springer Berlin Heidelberg, Berlin, Heidelberg, 1998, pp. 3–12, https://doi.org/10.1007/978-3-642-72106-9_1.

[37] A.A. MacDowell, D.Y. Parkinson, A. Haboub, E. Schaible, J.R. Nasiatka, C.A. Yee, J. R. Jameson, J.B. Ajo-Franklin, C.R. Brodersen, A.J. McElrone, X-Ray Micro-tomography at the Advanced Light Source, Proc.SPIE, 2012 850618, https://doi.org/10.1117/12.930243.

[38] G. Wolf, J. Lerchner, H. Schmidt, H. Gamsjager, E. Konigsberger, P.I. Schmidt, Thermodynamics of $CaCO_3$ Phase Transitions, vol. 46, 1996, pp. 353–359.

[39] G. Wolf, E. Königsberger, H.G. Schmidt, L.C. Königsberger, H. Gamsjäger, Thermodynamic aspects of the vaterite-calcite phase transition, J. Therm. Anal. Calorim. 60 (2000) 463–472, https://doi.org/10.1023/A:1010114131577.

[40] A.V. Radha, T.Z. Forbes, C.E. Killian, P.U.P.A. Gilbert, A. Navrotsky, Transformation and crystallization energetics of synthetic and biogenic amorphous calcium carbonate, Proc. Natl. Acad. Sci. U. S. A. 107 (2010) 16438–16443, https://doi.org/10.1073/pnas.1009959107.

[41] R.F. Feldman, Density and porosity studies of hydrated Portland cement, NRC Publ. Rec. 3 (1972) 5–14.

[42] J.R. Clifton, Some aspects of the setting and hardening of gypsum plaster, NBS Tech. Note 755 (1973) 1689–1699, https://doi.org/10.6028/NBS.TN.755.

[43] E. Badens, S. Veesler, R. Boistelle, Crystallization of gypsum from hemihydrate in presence of additives, J. Cryst. Growth 198–199 (1999) 704–709, https://doi.org/10.1016/S0022-0248(98)01206-8.

[44] C. Hargis, R. Gilliam, Compositions, Methods and Systems Related to Multi-Modal Distribution of Vaterite Particles, 2023. US20230339809A1.

[45] R.J. Gilliam, M. joseph Weiss, Methods and Systems for Forming Vaterite from Calcined Limestone Using Electric Kiln, 2022. US20220306483A1.

[46] K. Krugh, Paving the way for green cement commercialisation, Int. Cem. Rev. May (2024) 44–45.

[47] K. Krugh, Breaking New Ground Paving the Way for Green Cement Commercialization, Cem. Prod, 2024, pp. 20–21. April.